

# Volatility of organic aerosol and its components in the Megacity of Paris

Andrea Paciga<sup>a,b</sup>, Eleni Karnezi<sup>a,b</sup>, Evangelia Kostenidou<sup>c</sup>, Lea Hildebrandt<sup>d</sup>,  
Magda Psichoudaki<sup>c,e</sup>, Gabriella J. Engelhart<sup>b</sup>, Byong-Hyoek Lee<sup>b</sup>, Monica  
Crippa<sup>f,g</sup>, André S.H. Prévôt<sup>f</sup>, Urs Baltensperger<sup>f</sup>, and Spyros N. Pandis<sup>a,c,e</sup>

<sup>a</sup> Department of Chemical Engineering, Carnegie Mellon University, Pittsburgh, USA

<sup>b</sup> Center for Atmospheric Particle Studies, Carnegie Mellon University, Pittsburgh, USA

<sup>c</sup> Inst. of Chemical Engineering Sciences, FORTH/ICEHT, Patras, Greece

<sup>d</sup> McKetta Department of Chemical Engineering, University of Texas, Austin, USA

<sup>e</sup> Department of Chemical Engineering, University of Patras, Patras, Greece

<sup>f</sup> Laboratory of Atmospheric Chemistry, Paul Scherrer Institute, Villigen PSI, 5232, Switzerland

<sup>g</sup> European Commission, Joint Research Centre, Institute for Environment and Sustainability, Air and Climate  
Unit, Via Fermi, 2749, 21027 Ispra, Italy

## Abstract

Using a mass transfer model and the volatility basis set, we estimate the volatility distribution for the organic aerosol (OA) components during summer and winter in Paris, France as part of the collaborative project MEGAPOLI. The concentrations of the OA components as a function of temperature were measured combining data from a thermodenuder and an aerosol mass spectrometer (AMS) with Positive Matrix Factorization (PMF) analysis. The hydrocarbon-like organic aerosol (HOA) had similar volatility distributions for the summer and winter campaigns with half of the material in the saturation concentration bin of  $10 \mu\text{g m}^{-3}$  and another 35-40% consisting of low and extremely low volatility organic compounds (LVOCs with effective saturation concentrations  $C^*$  of  $10^{-3}$ - $0.1 \mu\text{g m}^{-3}$  and ELVOCs  $C^*$  less or equal than  $10^{-4} \mu\text{g m}^{-3}$ , respectively). The winter cooking OA (COA) was more than an order of magnitude less volatile than the summer COA. The low volatility oxygenated OA (LV-OOA) factor detected in the summer had the lowest volatility of all the derived factors and consisted almost exclusively of ELVOCs. The volatility for the semi-volatile oxygenated OA (SV-OOA) was significantly higher than that of the LV-OOA, containing both semi-volatile organic components (SVOCs with  $C^*$  in the  $1$ - $100 \mu\text{g m}^{-3}$  range) and LVOCs. The oxygenated OA (OOA) factor in winter consisted of SVOCs (45%), LVOCs (25%) and ELVOCs (30%). The volatility of marine OA (MOA) was higher than that of the other

35 factors containing around 60% SVOCs. The biomass burning OA (BBOA) factor  
36 contained components with a wide range of volatilities with significant contributions  
37 from both SVOCs (50%) and LVOCs (30%). Finally, combining the bulk average O:C  
38 ratios and volatility distributions of the various factors, our results are placed into the  
39 two-dimensional volatility basis set (2D-VBS) framework. The OA factors cover a broad  
40 spectrum of volatilities with no direct link between the average volatility and average  
41 O:C of the OA components.

42

### 43 **1. Introduction**

44 Atmospheric aerosols have adverse effects on human health (Caiazzo et al., 2013; Pope et  
45 al., 2009) and contribute to climate change (IPCC, 2013). Over 50% of the submicron  
46 particulate mass is often comprised of organic compounds (Zhang et al., 2007). OA  
47 (organic aerosol) originates from many different natural and anthropogenic sources and  
48 processes. It can be emitted directly, e.g., from fossil fuels and biomass combustion (so-  
49 called primary organic aerosol, POA) or can be formed by atmospheric oxidation of  
50 volatile, intermediate volatility and semi-volatile organic compounds (secondary organic  
51 aerosol, SOA). Since the oxidation pathways of organic vapors are complex and the  
52 corresponding reactions lead to hundreds or even thousands of oxygenated products for  
53 each precursor, our understanding of OA formation mechanisms and the OA chemical  
54 and physical properties remains incomplete. Furthermore, a lack of information regarding  
55 the sources along with the physical and chemical properties, and lifetime of organic  
56 aerosol (OA) has made predictions of OA concentrations by chemical transport models  
57 uncertain.

58 The volatility of atmospheric OA is one of its most important physical properties. It  
59 determines the partitioning of these organic compounds between the gas and particulate  
60 phases, the OA concentration, and the atmospheric fate of the corresponding compounds.  
61 Measurement of the OA volatility distribution has been recognized as one of the major  
62 challenges in our efforts to quantify the rates of formation of secondary organic  
63 particulate matter (Donahue et al., 2012). Thermodenuders (TD) have been developed to  
64 measure the volatility of ambient aerosol (Burtscher et al., 2001; Wehner et al., 2002,  
65 2004; Kalberer et al., 2004; An et al., 2007). Most TDs consist of two basic parts: a

66 heated tube where the more volatile particle components evaporate, leaving less volatile  
67 species behind and the denuder tube, usually containing activated carbon where the  
68 evaporated material is adsorbed thus avoiding potential re-condensation when the sample  
69 is cooled to room temperature. The aerosol mass fraction remaining (MFR) at a given  
70 temperature, after passing through the TD, is the most common way of reporting the TD  
71 measurements. The MFR, though an indirect metric of volatility for a specific TD  
72 operation, also depends on the aerosol concentration, size, enthalpy of vaporization,  
73 potential resistances to mass transfer, etc (Riipinen et al., 2010).

74 The two-dimensional volatility basis set (2D-VBS) framework from Donahue et al.  
75 (2012) has been used in order to describe atmospheric OA formation and evolution by  
76 lumping all organic compounds (with the exception of VOCs) into surrogates along two  
77 axes of volatility and the oxygen content (expressed as the O:C ratio or carbon oxidation  
78 state). Using the 2D VBS requires the ability to measure the OA distribution as a function  
79 of volatility and O:C ratio (or carbon oxidation state).

80 Positive Matrix Factorization (PMF), aims to deconvolve the bulk OA mass spectra  
81 obtained by the aerosol mass spectrometer (AMS) into individual “factors” that give  
82 information about the sources or processing of organic aerosol (Lanz et al., 2007; Ulbrich  
83 et al., 2009; Huffman et al., 2009; Zhang et al., 2011). Typical factors correspond to  
84 either primary sources including HOA (hydrocarbon-like OA), BBOA (biomass burning  
85 OA) and COA (cooking OA) or secondary OA like SV-OOA (semi-volatile oxygenated  
86 OA) and LV-OOA (low volatility oxygenated OA). Although there have been numerous  
87 studies that have identified PMF factors in ambient datasets, there have been few studies  
88 that have attempted to estimate the corresponding factor volatility (Huffman et al., 2009;  
89 Cappa and Jimenez, 2010). Huffman et al. (2009) characterized the volatility of PMF  
90 factors derived for the MILAGRO campaign in Mexico City and for the SOAR-1  
91 campaign in Riverside, CA. They concluded that BBOA was the most volatile and OOA  
92 was the least volatile component. HOA was more volatile than OOA in almost all cases.  
93 Cappa and Jimenez (2010), using a kinetic evaporation model, estimated the volatility  
94 distributions for the various PMF OA factors for the MILAGRO campaign. Here we  
95 extend this work focusing on another Megacity, Paris.

96 In this study, we estimate the volatility distributions of PMF factors derived from two  
97 month-long summer and winter campaigns in a suburban background site in Paris. The  
98 data analysis approach is first outlined and the corresponding challenges are discussed.  
99 We use the mass transfer model of Riipinen et al. (2010), together with the approach  
100 introduced by Karnezi et al. (2014) to estimate the volatility distributions for all PMF  
101 factors. We finally synthesize the corresponding OA findings using the 2D-VBS  
102 framework.

## 103 **2. Methods**

### 104 *2.1 Measurement Site and Sampling*

105 Two comprehensive field campaigns were performed during July of 2009 and  
106 January/February of 2010 at an urban background sampling site, SIRTa (Site  
107 Instrumental de Recherche par Teledetection Atmospherique) (Haefelin et al., 2005)  
108 located about 20 km southwest of Paris' city center. The datasets were collected as part of  
109 a collaborative project known as MEGAPOLI (Megacities: Emissions, urban, regional,  
110 and Global Atmospheric POLution and climate effects, and Integrated tools for  
111 assessment and mitigation) (Baklanov et al., 2008; Beekmann et al., 2015). A suite of  
112 instruments were used including a high-resolution time-of-flight aerosol mass  
113 spectrometer (HR-ToF-AMS) from Aerodyne research, Inc. (DeCarlo et al., 2006) for  
114 particle mass and composition, a scanning mobility particle sizer (SMPS) from TSI, Inc.  
115 for particle size and number distributions and the Carnegie Mellon University  
116 thermodenuder (TD) for volatility measurements.

117

118 The TD design was similar to that described in An et al. (2007), consisting of a heated  
119 tube followed by a denuding section, which uses activated charcoal to prevent  
120 recondensation of organic vapors. The TD was operated at temperatures ranging from  
121 about 20°C to 200°C during both campaigns, yielding thermograms of the organic  
122 aerosol mass remaining as a function of TD temperature. The TD scanned this  
123 temperature range using different temperatures each day. A centerline residence time of  
124 25 s at 298 K was used for all measurements (Lee et al., 2010). This corresponds to mean  
125 residence time of approximately 50 s at 298 K.

126 Changes in composition, mass, and size as a result of aerosol evaporation were quantified  
127 by both the SMPS and the HR-ToF-AMS by alternate sampling between the TD and the  
128 ambient sample line, every 5 minutes. The SMPS was operated with a sheath flow of 5 L  
129  $\text{min}^{-1}$  and a sample flow rate of 0.5 L  $\text{min}^{-1}$ . The HR-ToF-AMS, which measures the  
130 aerosol size-composition distribution of the submicron non-refractory material, was  
131 operated in both the higher sensitivity mode (V-mode) and the higher resolution mode  
132 (W-mode) (DeCarlo et al., 2006). The V-mode data are used in this study. The AMS  
133 collection efficiency was estimated at 0.38 during the summer (Crippa et al., 2013a) and  
134 0.5 during the winter (Crippa et al., 2013b).

135

## 136 *2.2 Data Analysis*

137 TD raw measurements need to be corrected for particle losses due to diffusion of small  
138 particles, sedimentation of larger particles, and thermophoretic losses (Burtcher et al.,  
139 2001). To account for these losses, which depend on particle size, TD temperature, and  
140 sample flow rate, Lee (2010) has developed size and temperature dependent corrections  
141 for this particular TD. The organic aerosol concentrations measured after the TD were  
142 corrected for losses corresponding to the operating conditions during the campaign. The  
143 OA mass fraction remaining (MFR) was calculated dividing the loss-corrected OA  
144 concentration after the TD at time period  $i$  with that of the by-pass line at time period  $i+1$ .  
145 The fact that the two measurements correspond to two different 5 min time intervals  
146 introduces some uncertainty in the calculated MFR values because of the variability of  
147 the atmospheric concentrations. Some of this variability is averaged out when average  
148 MFR values are calculated for each temperature.

149 The preparation of these large datasets for analysis required careful examination of the  
150 ambient OA variability in order to determine the appropriate averaging intervals. The OA  
151 mass concentration data for the summer campaign is shown in Figure 1. Overall, the  
152 particulate matter mass concentration was surprisingly low during this period in Paris,  
153 with a campaign average  $\text{PM}_{10}$  OA for SIRTAs of only  $0.83 \mu\text{g m}^{-3}$ . As expected, there  
154 were several periods during which the OA concentration was much higher than  $1 \mu\text{g m}^{-3}$   
155 reaching levels up to  $6 \mu\text{g m}^{-3}$ . To evaluate whether the OA during these higher

156 concentration periods had different MFR values than the rest of the samples, we  
157 separated the data in two groups using an OA concentration cutoff of  $1.5 \mu\text{g m}^{-3}$ . Figure  
158 S1 in the supplementary information shows the corresponding MFR measurements for  
159 both low and high concentration periods. Given the experimental variability, there is no  
160 discernable difference in evaporation between the higher and the lower concentration  
161 periods and therefore, these were averaged together for the analysis. The similarity of the  
162 average MFR values during these low and high concentration periods (the latter were  
163 often characterized by higher OA variability) also suggests that our calculation of the  
164 MFR using measurement pairs did not introduce significant bias in the average estimated  
165 MFR.

166 We performed a similar analysis for the winter campaign. Paris during winter, unlike the  
167 summer, was characterized by higher fine PM concentrations with an average  $\text{PM}_{10}$  OA  
168 concentration of  $3.1 \mu\text{g m}^{-3}$  (Figure 2). The OA threshold concentration was chosen to be  
169  $4.5 \mu\text{g m}^{-3}$  and again there was no evidence of effects of concentration (in the observed  
170 range) on volatility (Supplementary Information, Fig. S2) and the corresponding MFRs  
171 were averaged together. Finally, the data points were averaged into temperature bins of  
172  $5^\circ\text{C}$ . The calculation of one MFR value every  $5^\circ\text{C}$  is a compromise between the need to  
173 average more data points at similar temperatures and maintaining the dynamic behavior  
174 of the thermogram. Averaging over wider temperature ranges (e.g.  $10^\circ\text{C}$ ) did not result in  
175 any essential differences in our analysis and conclusions.

176 Along with the bulk organic measurements, additional information can be derived from  
177 the HR-ToF-AMS V-mode mass spectra using the PMF analysis technique. The  
178 deconvolved spectra yielded several organic aerosol “factors” for each campaign. A  
179 complete discussion of the PMF analysis of the ambient measurements and the resulting  
180 factors can be found in Crippa et al. (2013a; b). The PMF analysis was repeated,  
181 combining both ambient and thermodenuded spectra with guidance from the original  
182 analysis of the ambient-only data (e.g., the same number of factors was used). This  
183 second analysis produced for all practical purposes the same results for the ambient data  
184 set as that of the ambient measurements only and can be found in the corresponding  
185 publications.

186 The low OA concentrations especially during the summer resulted in very low  
187 concentrations of the corresponding factors and thus high MFR uncertainty. The MFRs of  
188 the various factors were, as expected, extremely variable when the factor concentrations  
189 were close to zero. Therefore, to minimize these problems, a minimum ambient mass  
190 concentration was determined for each PMF factor, based on the concentration range for  
191 which MFR measurements exceeded 1.5. The average ambient concentration and  
192 threshold concentration with corresponding statistical information for each PMF factor is  
193 shown in Table 1. The corresponding factor concentration thresholds during the summer  
194 were in the 0.05-0.1  $\mu\text{g m}^{-3}$  range. MFR measurements of PMF factors with ambient  
195 levels less than 0.1  $\mu\text{g m}^{-3}$  are clearly quite uncertain. All the corresponding MFR values  
196 from these low factor concentration periods were excluded from the analysis. Few MFR  
197 measurements were excluded during the winter period, while 20-50% of the  
198 measurements for the various factors were excluded during the summer.

199

### 200 *2.3 Volatility Distribution Estimation*

201 To estimate the volatility distributions from the corrected thermograms we employed the  
202 dynamic mass transfer model of Riipinen et al. (2010). The model simulates particle  
203 evaporation using experimental inputs including TD temperature and residence time,  
204 initial particle size, and ambient OA concentration. The volatility of these complex  
205 mixtures is defined using the corresponding effective saturation concentration,  $C^*$ , at 298  
206 K. Along with saturation concentration, two parameters that can affect the evaporation  
207 rate and the corresponding volatility estimation are the enthalpy of vaporization and the  
208 mass accommodation coefficient. Unfortunately, these values are currently unknown for  
209 these complex multi-component systems. Often, a mass accommodation coefficient of  
210 unity is assumed. However, mass transfer limitations to evaporation have been observed  
211 in some experimental systems, leading to mass accommodation coefficient values of  
212 much less than one (Saleh et al., 2013). Typical values of 100  $\text{kJ mol}^{-1}$  and 1.0 are  
213 assumed for the enthalpy of vaporization and accommodation coefficient, respectively.  
214 Use of lower accommodation coefficient values results in shifting of the estimated  
215 volatility distributions to higher values. Lee et al. (2010) explored this sensitivity and  
216 estimated that an order of magnitude change in the mass accommodation coefficient was

217 “equivalent” to a corresponding change in the volatility distribution. Similar conclusions  
218 about the sensitivity of the estimated volatility to the accommodation coefficient were  
219 reached by Cappa and Jimenez (2010) as well as Riipinen et al. (2010).

220 As described in Donahue et al. (2006), the volatility distribution is represented by  
221 surrogate species with a saturation concentration of  $C_i^*$ . The  $C_i^*$  bins are logarithmically  
222 spaced, allowing for extremely low and high volatility species to be compared in a single  
223 framework. The analysis here was limited to a 6-consecutive  $C^*$  bin solution with a  
224 variable mass fraction value for each bin. Different volatility ranges were tested and the  
225 best range was selected for each factor. The “goodness of fit” was quantified using the  
226 error analysis outlined in Karnezi et al. (2014). The standard error was calculated for all  
227  $C^*$  bin-mass fraction combinations. For a given 6-bin solution, the top 2% of mass  
228 fraction combinations with the lowest error was used to find the average mass fraction in  
229 each bin and the corresponding standard deviation.

230 The OA components are described as semi-volatile (SVOCs with  $C^*$  of 1, 10, and 100  $\mu\text{g m}^{-3}$ ),  
231 low volatility (LVOCs with  $C^*$  of  $10^{-3}$ ,  $10^{-2}$ , and  $0.1 \mu\text{g m}^{-3}$ ), and extremely low  
232 volatility (ELVOCs with  $C^* \leq 10^{-4} \mu\text{g m}^{-3}$ ) in the rest of the paper (Murphy et al., 2014).

233

### 234 **3. Results and Discussion**

#### 235 *3.1 Organic Aerosol Volatility*

236 The average loss-corrected OA thermograms for the two seasons are shown in Figure 3.  
237 The two thermograms seem very similar while differences are mostly noticeable at the  
238 high temperatures. In the winter thermogram an approximate 30% remained at 180°C  
239 while in the summer thermogram less than 10% was present at the same temperature.  
240 This might suggest more ELVOCs being present at winter. However, the summer  
241 thermogram shows that nearly 50% of the mass evaporated at a thermodenuder  
242 temperature of 83 °C ( $T_{50}$ ). The winter measurements suggested a similar  $T_{50}$  value of 88  
243 °C. This crude comparison of volatility through the corresponding thermograms suggests  
244 that the OA in the two seasons could have similar average volatility distributions. It is  
245 surprising that the seasonal differences in emissions are not reflected in the corresponding

246 thermograms. We will examine the reasons for this similarity in the subsequent section  
247 by analyzing the volatility of the corresponding factors.

248

249 The volatility distributions for the total OA for the two seasons are depicted in Figure 4.  
250 They are quite similar to each other especially considering the corresponding  
251 uncertainties and they are characterized by higher concentrations of components with  
252  $C^*=10^{-4}$  and  $10 \mu\text{g m}^{-3}$ .

253

### 254 *3.2 Volatility of Organic Aerosol Components*

255 Five PMF factors were determined for the summer dataset by Crippa et al. (2013a).  
256 Hydrocarbon-like OA (HOA) most closely resembles fresh vehicle emissions in that the  
257 mass spectrum resembles that of transportation sources. Cooking OA (COA) was also  
258 observed in the summer campaign, peaking during noon and evening meal times. Marine  
259 OA (MOA) was identified based on relatively high levels of organic sulfur and a strong  
260 correlation with methanesulfonic acid (MSA), which is a product of continued oxidation  
261 of phytoplankton decomposition products. Two SOA factors were also reported: Semi-  
262 volatile oxygenated OA (SV-OOA) and low volatility oxygenated OA (LV-OOA). These  
263 two factors were differentiated based on their O:C ratio. The two secondary OA factors  
264 made up 57% of the total OA mass. The remaining factors contributed fairly similar  
265 average fractions of 18% for COA, 12% for HOA, and 13% for MOA. Detailed  
266 discussion of the PMF factors along with verification analysis were provided by Crippa et  
267 al. (2013a).

268

269 The PMF analysis for the winter campaign yielded four factors. The HOA and COA  
270 factors were again present. There was also a single secondary OA factor which was  
271 termed oxygenated OA (OOA). This factor could not be further separated into SV-OOA  
272 and LV-OOA. The final factor reported was biomass burning OA (BBOA), correlating  
273 with known molecular markers for residential wood burning (e.g., levoglucosan). The  
274 OOA factor was found to dominate the organic aerosol mass, contributing nearly 65% on

275 average. The complete analysis and description of these factors can be found in Crippa et  
276 al. (2013b).

277

278 Using the mass transfer model from Riipinen et al. (2010) and the approach of Karnezi et  
279 al. (2014) we fitted the corresponding thermograms (Figure S3), using a  $C^*$  bin solution  
280 with a variable mass fraction value for each bin. Specifically for each factor we used an  
281 individual consecutive 6-bin solution (chosen as the 6-bin solution with the best fits)  
282 resulting in the volatility distributions, shown in Figure 5. The modeled thermograms for  
283 all factors from both summer and winter campaigns are shown in Figure 6. Finally, the  
284 volatility distributions for each factor are summarized in Table S1 in the supplementary  
285 information. The fitting of individual factor thermograms implicitly assumes that each  
286 factor had the same size distribution as the total OA and that the factors were present as  
287 an external mixture. To test the uncertainty introduced by this assumption we compared  
288 the volatility distribution of the total OA with the composition weighted sum of the  
289 volatility distributions of the individual OA factors for both summer and winter. The two  
290 distributions (total and sum of factors) agreed within a few percent for both seasons  
291 suggesting that the uncertainty is modest and within the uncertainty limits shown in the  
292 corresponding figures.

293

294 The HOA factors for the summer and winter campaigns had very similar thermograms  
295 and volatility distributions with half of the material in the  $10 \mu\text{g m}^{-3}$  bin (Figure 5).  
296 Roughly 40% of the HOA in both seasons consisted of LVOCs and ELVOCs. This  
297 volatility similarity is consistent with the similarity in mass spectra derived by the PMF  
298 analysis (Figure 7a). The angle  $\theta$  between the corresponding vectors (treating the AMS  
299 spectra as vectors according to Kostenidou et al. (2009)) was  $14^\circ$  suggesting similar  
300 chemical fingerprints. This is not surprising for a Megacity where the transportation and  
301 any industrial sources are expected to have chemically similar emissions in both summer  
302 and winter. Similar were also the  $T_{50}$  for the HOA factors with values of  $49^\circ\text{C}$  and  $54^\circ\text{C}$   
303 for the summer and winter campaign, respectively. Cappa and Jimenez (2010) also  
304 estimated that the HOA in Mexico City had a wide volatility distribution with  
305 approximately 35% of its mass consisting of LVOCs and ELVOCs while the remaining

306 65% was SVOCs. Almost 40% of the HOA had  $C^* \geq 10 \mu\text{g m}^{-3}$  which compares very  
307 well with the 50% estimated here.

308

309 The situation was quite different for the cooking OA factor. Here the seasonal differences  
310 were more pronounced for the thermograms (Fig. 6), the estimated volatility distributions  
311 (Fig. 5) and the corresponding mass spectra (Fig. 7b). The winter COA was substantially  
312 less volatile than the summer COA, more than an order of magnitude based on average  
313  $\log C^*$  values, weighted by the mass fraction of each bin (average  $C^* = 10^{-2} \mu\text{g m}^{-3}$  for the  
314 summer campaign and average  $C^* = 4 \times 10^{-4} \mu\text{g m}^{-3}$  for the winter campaign). The COA  
315 factor during the winter campaign did not contain semi-volatile components while 37%  
316 of the summer COA was semi-volatile. The COA winter factor consisted of ELVOCs  
317 (37%) and LVOCs (63%). The COA mass spectra in Figure 7b show that the winter COA  
318 was characterized by a higher fraction of molecular fragments at higher mass-to-charge  
319 ( $m/z$ ) ratio. This is consistent with organic components of longer carbon chain which, for  
320 the same level of oxidation, are expected to have lower volatility. The angle  $\theta$  between  
321 the COA spectra was  $26^\circ$ , suggesting a significant chemical difference. One explanation  
322 is that the cooking habits are different in the two seasons with outdoor cooking (e.g.,  
323 barbecue) dominating in the summer and indoor cooking relying more on oil and butter,  
324 being more significant in the winter. We also cannot rule out some imperfect unmixing of  
325 OA sources and components. The  $T_{50}$  for the COA factors were different as well, with  
326 values of  $91^\circ\text{C}$  and  $148^\circ\text{C}$  for the summer and winter campaign, respectively.

327 The LV-OOA factor detected in the summer had the lowest volatility (Fig. 5) of all the  
328 derived factors. There was no sign of evaporation until the TD temperature reached  
329 nearly  $150^\circ\text{C}$  (Fig. 6). We estimate that this factor consisted almost exclusively of OA  
330 with effective saturation concentrations equal to or lower than  $10^{-3} \mu\text{g m}^{-3}$ , which are  
331 almost exclusively ELVOCs. The average ambient concentration of this factor during the  
332 summer was  $0.12 \mu\text{g m}^{-3}$  and its average  $C^*$  was equal to  $5 \times 10^{-6} \mu\text{g m}^{-3}$ . Very low  
333 volatilities (practically all the OA had  $C^* \leq 10^{-3} \mu\text{g m}^{-3}$ ) were also estimated for LV-  
334 OOA by Cappa and Jimenez (2010) in Mexico City during the MILAGRO campaign.

335 The estimated volatility for the SV-OOA factor is consistent with its naming by Crippa et  
336 al. (2013a) as it was significantly higher than that of the LV-OOA (Fig. 5). We estimated  
337 that roughly half of the SV-OOA was SVOCs while it contained also LVOCs (42%) and  
338 a small amount of ELVOCs (6%). Its  $T_{50}$  was 61 °C and its average  $C^*$  was roughly 0.2  $\mu\text{g}$   
339  $\text{m}^{-3}$ . These values are once more generally consistent with the estimates of Cappa and  
340 Jimenez (2010) showing that SVOCs dominated the SV-OOA during MILAGRO  
341 (approximately 40%) with LVOCs contributing another 35%.

342 The OOA factor determined in the winter had a volatility distribution (Fig. 5), containing  
343 SVOCs (45%), LVOCs (25%) and ELVOCs (30%). The winter OOA and the summer  
344 SV-OOA spectra had a  $\theta$  angle of 34°, while there was an even larger discrepancy  
345 between the winter OOA and the summer LV-OOA with an angle of 37°. The  $T_{50}$  was  
346 equal to 85°C. These differences in mass spectra and  $T_{50}$  are consistent with the  
347 differences in volatility. The average volatility of OOA was much higher than LVOOA in  
348 summer but lower than SVOOA.

349 The marine OA (MOA) factor was only detected during the summer campaign at an  
350 average concentration of 0.17  $\mu\text{g m}^{-3}$ . Its volatility was relatively high (Fig. 6), and  
351 almost all the MOA had evaporated at 100 °C. The MOA factor consisted mainly of  
352 SVOCs (61%) and some LVOCs (36%). Its  $T_{50}$  was equal to 58 °C and its average  $C^*$  was  
353 approximately 0.4  $\mu\text{g m}^{-3}$ .

354 The BBOA factor was present in the winter dataset with an average ambient  
355 concentration of 0.6  $\mu\text{g m}^{-3}$ . The corresponding estimated volatility distribution (Fig. 5)  
356 shows that half of the BBOA factor consisted of SVOCs (with most material in the 10  $\mu\text{g}$   
357  $\text{m}^{-3}$  bin) and the other half of LVOCs and ELVOCs. A similar bimodal distribution was  
358 also found by May et al. (2013) with a peak at 0.01 and one at 100  $\mu\text{g m}^{-3}$  for controlled  
359 biomass burning in the laboratory. The difference in the location of the high volatility  
360 peak can potentially be explained by the wider range of concentrations in the experiments  
361 analyzed by May et al. (2013) compared to the limited range in the ambient Paris  
362 measurements. The more volatile BBOA components were never in the particulate phase  
363 in our dataset so their abundance cannot be determined. The BBOA  $T_{50}$  was 70 °C, higher

364 than that of HOA and less than those of COA and OOA. Finally, its average  $C^*$  was  
365 approximately  $0.1 \mu\text{g m}^{-3}$ . The BBOA in Mexico City was approximately half LVOCs  
366 and half SVOCs (Cappa and Jimenez, 2010) and had a much lower ELVOC fraction than  
367 the wintertime Paris BBOA in the present study.

368

#### 369 **4. Synthesis of Results in the 2D-VBS**

370 We employed the 2-D VBS framework in order to synthesize the above results,  
371 combining the bulk average O:C ratio and volatility distributions of the various factors.  
372 Each of the different factors had a distribution of O:C values, but this distribution cannot  
373 be determined from the AMS measurements. The HOA, BBOA, and COA factors all had  
374 relatively low O:C values but they covered a wide range of average volatilities (Fig. 8).  
375 The MOA and secondary OA factors for both seasons had much higher O:C values but  
376 they also covered a wide range of volatilities, with LV-OOA having the lowest one. The  
377 HOA during summer had higher O:C than HOA during winter, suggesting incomplete  
378 separation from aged HOA or difference in the sources, while their volatility distribution  
379 was similar, as discussed earlier. The COA factor during the summer campaign, had  
380 slightly higher O:C and a higher volatility than the COA from the winter campaign. The  
381 OOA during the winter had the highest O:C ratio but compared to the less oxidized  
382 SVOOA, it had lower average volatility and higher volatility compared to LVOOA.  
383 These results indicate that there was not a direct link between the average volatility and  
384 the bulk average O:C for these OA components. This is actually the reason for the  
385 introduction of the 2D-VBS: the second dimension is needed to capture at least some of  
386 the chemical complexity of the multitude of organic compounds in atmospheric  
387 particulate matter.

388

389 The broad spectrum of volatilities and extent of oxidation are not surprising. Donahue et  
390 al. (2012) extrapolated from the few available ambient measurements to provide rough  
391 estimates of the factor locations on the 2D-VBS. Superimposition of our factors and those  
392 estimated by Donahue et al. (2012) (Fig S4) indicates that the factor locations agree  
393 surprisingly well. This is quite encouraging both for our results and our current  
394 understanding of the evolution of atmospheric OA.

## 395 **5. Conclusions**

396 Two month-long field campaigns were conducted at an urban background sampling site,  
397 SIRTA in Paris, France as part of the collaborative project MEGAPOLI. The particulate  
398 matter mass concentration was surprisingly low during summer in Paris, with a campaign  
399 average PM<sub>1</sub> OA for SIRTA of only 0.83 μg m<sup>-3</sup>, while during winter it was characterized  
400 by higher fine PM concentrations, with an average PM<sub>1</sub> OA concentration of 3.1 μg m<sup>-3</sup>.

401 The volatility distributions of PMF factors derived during both campaigns were  
402 estimated. Five factors were determined for the summer dataset. Hydrocarbon-like OA  
403 (HOA), cooking OA (COA), marine OA (MOA) and two Secondary OA (SOA) factors  
404 were also identified: Semi-volatile oxygenated OA (SV-OOA) and low volatility  
405 oxygenated OA (LV-OOA). The PMF analysis for the winter campaign determined four  
406 factors. The HOA and COA factors were again identified. There was also a single  
407 secondary OA factor that was termed oxygenated OA (OOA). The final factor observed  
408 was biomass burning OA (BBOA).

409 The HOA factors for both campaigns had similar volatility distributions with half  
410 material in the 10 μg m<sup>-3</sup> bin. Both factors contained also LVOCs and ELVOCs with a  
411 total contribution of around 40% to the HOA mass. This similarity was consistent with  
412 the corresponding mass spectra derived by the PMF analysis.

413 The summer COA was significantly more volatile than the winter COA. The weighted-  
414 average COA C\* during the summer was more than order of magnitude higher than that  
415 in the winter. The winter COA did not contain any semi-volatile organic components  
416 (SVOCs) whereas 37% of the summer COA was semi-volatile. LVOCs were significant  
417 components of the COA, representing 37% of the COA in the summer and 63% in the  
418 winter. These differences in volatility were consistent with the differences in AMS  
419 spectra and could be due to different seasonal cooking habits. Also, imperfect separation  
420 of the OA components by PMF cannot be excluded.

421 The LV-OOA factor detected in the summer had the lowest volatility of all the derived  
422 factors. There was no sign of LV-OOA evaporation until the TD temperature reached 150

423 °C. The LV-OOA factor consisted nearly exclusively of ELVOCs (97%). Roughly half of  
424 the SV-OOA mass consisted of SVOCs while the rest was mainly LVOCs (42%). The  
425 OOA factor determined in the winter had a volatility distribution containing SVOCs  
426 (45%), ELVOCs (30%) and LVOCs (25%).

427 The marine OA (MOA) factor, only detected during the summer campaign, was relatively  
428 volatile with an average  $C^*$  of approximately  $0.4 \mu\text{g m}^{-3}$ . The MOA factor consisted  
429 mainly of SVOCs (61%) and LVOCs (36%).

430 The BBOA factor was present in winter with an average ambient concentration of  $0.6 \mu\text{g}$   
431  $\text{m}^{-3}$ . Half of the BBOA consisted of SVOCs and the other half of extremely low volatile  
432 and low volatile organic components. The BBOA was less volatile than the HOA factors  
433 but more volatile than COA and OOA.

434 Finally, combining the O:C ratio and volatility distributions of the various factors, we  
435 integrated our results into the 2D-VBS synthesizing the corresponding OA findings. The  
436 factor locations agreed well with the location of factors proposed by Donahue et al.  
437 (2012). The HOA, BBOA, and COA factors had all relatively low O:C but their average  
438 volatilities were different by orders of magnitude. The MOA for summer and secondary  
439 OA factors for both seasons had much higher O:C with a wide variety of volatilities,  
440 where MOA had the highest one and LV-OOA had the lowest one. The results suggest  
441 that the average O:C factor was not directly linked to its average volatility, underlining  
442 the importance of measuring both properties, and that all factors include compounds with  
443 a wide range of volatilities.

444 The estimated volatility distributions by the use of just TD measurements are  
445 characterized by considerable uncertainties (Karnezi et al., 2014). However, the relative  
446 volatilities of the various factors discussed above should be more robust. The absolute  
447 volatility distributions do depend on the assumed enthalpy of vaporization and  
448 accommodation coefficient (parameterization of mass transfer resistances). They also  
449 depend on the assumptions of similar size distributions and external mixing of the OA  
450 components corresponding to each factor.

451 **Acknowledgements**

452 This research was supported by the FP7 project MEGAPOLI, the FP7 IDEAS project  
453 ATMOPACS, and the ESF-NRSF ARISTEIA grant ROMANDE. Lea Hildebrandt was  
454 supported by a Graduate Research Fellowship from the United States National Science  
455 Foundation.

456

457 **6. References**

458 An, W. J., Pathak, R. K., Lee, B.-H. and Pandis, S. N.: Aerosol volatility measurement  
459 using an improved thermodenuder: Application to secondary organic aerosol,  
460 Journal of Aerosol Science, 38, 305–314, doi:10.1016/j.jaerosci.2006.12.002,  
461 2007.

462 Baklanov, A., Lawrence, M. G. and Pandis, S. N.: Description of work document for the  
463 European Collaborative Project “Megacities: Emissions, urban, regional and  
464 Global Atmospheric POLLution and climate effects, and Integrated tools for  
465 assessment and mitigation” (MEGAPOLI) for the Seventh Framework  
466 Programme of the European Commission, <http://megapoli.info>, 2008.

467 Beekmann, M., Prévôt, A. S. H., Drewnick, F., Sciare, J., Pandis, S. N., Denier van der  
468 Gon, H. A. C., Crippa, M., Freutel, F., Poulain, L., Gherzi, V., Rodriguez, E.,  
469 Beirle, S., Zotter, P., von der Weiden-Reinmuller, S. L., Bressi, M., Fountoukis,  
470 C., Petetin, H., Szidat, S. Schneider, J., Rosso, A., El Haddad, I., Megaritis, A.,  
471 Zhang, Q. J., Michoud, V., Slowik, J. G., Moukhtar, S., Kolmonen, P., Stohl, A.,  
472 Eckardt, S., Borbon, A., Gros, V., Marchand, N., Jaffrezo, J. L., Schwarzenboeck,  
473 A., Colomb, A., Wiedensohler, A., Borrmann, S., Lawrence, M., Baklanov, A.,  
474 and Baltensperger, U. (2015). In-situ, satellite measurement and model evidence  
475 for a dominant regional contribution to fine particulate matter levels in the Paris  
476 Megacity, Atmospheric Chemistry and Physics Discussions, 15, 8647-8686.

477 Burtscher, H., Baltensperger, U., Bukowiecki, N., Cohn, P., Hüglin, C., Mohr, M.,  
478 Matter, U., Nyeki, S., Schmatloch, V. and Streit, N.: Separation of volatile and  
479 non-volatile aerosol fractions by thermodesorption: instrumental development and  
480 applications, Journal of Aerosol Science, 32, 427–442, 2001.

481 Caiazzo, F., Ashok, A., Waitz, I. A., Yim, S. H. L. and Barrett, S. R. H.: Air pollution

482 and early deaths in the United States. Part I: Quantifying the impact of major  
483 sectors in 2005, *Atmospheric Environment*, 79, 198–208,  
484 doi:10.1016/j.atmosenv.2013.05.081, 2013.

485 Cappa, C. D. and Jimenez, J. L.: Quantitative estimates of the volatility of ambient  
486 organic aerosol, *Atmos. Chem. Phys.*, 10, 5409–5424, doi:10.5194/acp-10-5409-  
487 2010, 2010.

488 Crippa, M., Haddad, El, I., Slowik, J. G., DeCarlo, P. F., Mohr, C., Heringa, M. F.,  
489 Chirico, R., Marchand, N., Sciare, J., Baltensperger, U. and Prévôt, A. S. H.:  
490 Identification of marine and continental aerosol sources in Paris using high  
491 resolution aerosol mass spectrometry, *J. Geophys. Res. Atmos.*, 118, 1950–1963,  
492 doi:10.1002/jgrd.50151, 2013a.

493 Crippa, M., DeCarlo, P. F., Slowik, J. G., Mohr, C., Heringa, M. F., Chirico, R., Poulain,  
494 L., Freutel, F., Sciare, J., Cozic, J., Di Marco, C. F., Elsasser, M., Nicolas, J. B.,  
495 Marchand, N., Abidi, E., Wiedensohler, A., Drewnick, F., Schneider, J.,  
496 Borrmann, S., Nemitz, E., Zimmermann, R., Jaffrezo, J. L., Prévôt, A. S. H. and  
497 Baltensperger, U.: Wintertime aerosol chemical composition and source  
498 apportionment of the organic fraction in the metropolitan area of Paris, *Atmos.*  
499 *Chem. Phys.*, 13, 961–981, doi:10.5194/acp-13-961-2013, 2013b.

500 DeCarlo, P. F., Kimmel, J. R., Trimborn, A., Northway, M. J., Jayne, J. T., Aiken, A. C.,  
501 Gonin, M., Fuhrer, K., Horvath, T., Docherty, K. S., Worsnop, D. R. and Jimenez,  
502 J. L.: Field-deployable, high-resolution, time-of-flight aerosol mass spectrometer,  
503 *Anal. Chem.*, 78, 8281–8289, doi:10.1021/ac061249n, 2006.

504 Donahue, N. M., Robinson, A. L., Stanier, C. O. and Pandis, S. N.: Coupled partitioning,  
505 dilution, and chemical aging of semivolatile organics, *Environ. Sci. Technol.*, 40,  
506 2635–2643, doi:10.1021/es052297c, 2006.

507 Donahue, N. M., Kroll, J. H., Pandis, S. N. and Robinson, A. L.: A two-dimensional  
508 volatility basis set – Part 2: Diagnostics of organic-aerosol evolution, *Atmos.*  
509 *Chem. Phys.*, 12, 615–634, doi:10.5194/acp-12-615-2012, 2012.

510 Haefelin, M., Barthès, L., Bock, O., Boitel, C., Bony, S., Bouniol, D., Chepfer, H.,  
511 Chiriac, M., Cuesta, J., Delanoë, J., Drobinski, P., Dufresne, J. L., Flamant, C.,  
512 Grall, M., Hodzic, A., Hourdin, F., Lapouge, F., Lemaître, Y., Mathieu, A.,

513 Morille, Y., Naud, C., Noël, V., O'Hirok, W., Pelon, J., Pietras, C., Protat, A.,  
514 Romand, B., Scialom, G. and Vautard, R.: SIRTA, a ground-based atmospheric  
515 observatory for cloud and aerosol research, *Ann. Geophys.*, 23, 253–275,  
516 doi:10.5194/angeo-23-253-2005, 2005.

517 Huffman, J. A., Docherty, K. S., Aiken, A. C., Cubison, M. J., Ulbrich, I. M., DeCarlo, P.  
518 F., Sueper, D., Jayne, J. T., Worsnop, D. R., Ziemann, P. J. and Jimenez, J. L.:  
519 Chemically-resolved aerosol volatility measurements from two megacity field  
520 studies, *Atmos. Chem. Phys.*, 9, 7161–7182, 2009.

521 IPCC: Climate Change: The Physical Science Basis – Contribution of Working Group I  
522 to the Fifth Assessment Report of the Intergovernmental Panel on Climate  
523 Change, edited by: Stocker, T.F., Qin, D., Plattner, G.K., Tignor, M., Allen, S.K.,  
524 Boschung, J., Nauels, A., Xia, Y., Bex, V., and Midgley, P.M. (eds.), Cambridge  
525 University Press, Cambridge, United Kingdom and New York, NY, USA, 1535  
526 pp., 2013.

527 Kalberer, M., Paulsen, D., Sax, M., Steinbacher, M., Dommen, J., Prevot, A. S. H.,  
528 Fisseha, R., Weingartner, E., Frankevich, V., Zenobi, R., and Baltensperger, U.:  
529 Identification of polymers as major components of atmospheric organic aerosols,  
530 *Science*, 303, 1659–1662, 2004.

531 Karnezi, E., Riipinen, I. and Pandis, S.N. : Measuring the atmospheric organic aerosol  
532 volatility distribution: a theoretical analysis, *Atmos. Meas. Tech.*, 7, 2953–2965,  
533 2014.

534 Kostenidou, E., Lee, B. H., Engelhart, G. J., Pierce, J. R., and Pandis, S. N.: Mass spectra  
535 deconvolution of low, medium and high volatility biogenic secondary organic  
536 aerosol, *Environ. Sci. Technol.*, 43, 4884–4889, 2009.

537 Lanz, V. A., Alfarra, M. R., Baltensperger, U., Buchmann, B., Hueglin, C. and Prévôt, A.  
538 S. H.: Source apportionment of submicron organic aerosols at an urban site by  
539 factor analytical modelling of aerosol mass spectra, *Atmos. Chem. Phys.*, 7,  
540 1503–1522, 2007.

541 Lee, B.H., Kostenidou, E., Hildebrandt, L., Riipinen, I., Engelhart, G.J., Mohr, C.,  
542 DeCarlo, P.F., Mihalopoulos, N., Prevot, A.S.H., Baltensperger, U., Pandis, S.N.:  
543 Measurement of the ambient organic aerosol volatility distribution: application

544 during the Finokalia Aerosol Measurement Experiment (FAME-2008), *Atmos.*  
545 *Chem. Phys.*, 10, 12149-12160, doi: 10.5194/acp-10-12149-2010, 2010.

546 May, A. A., Levin, E. J. T., Hennigan, C. J., Riipinen, I., Lee, T., Collett, J. L., Jr.,  
547 Jimenez, J. L., Kreidenweis, S. M. and Robinson, A. L.: Gas-particle partitioning  
548 of primary organic aerosol emissions: 3. Biomass burning, *J. Geophys. Res.*  
549 *Atmos.*, 118, 11,327–11,338, doi:10.1002/jgrd.50828, 2013.

550 Murphy, B. N., Donahue, N. M., Robinson, A. L., and Pandis, S. N.: A naming  
551 convention for atmospheric organic aerosol, *Atmos. Chem. Phys.*, 14, 5825-5839,  
552 doi:10.5194/acp-14-5825-2014, 2014.

553 Pope, C. A., III, Ezzati, M. and Dockery, D. W.: Fine-particulate air pollution and life  
554 expectancy in the United States, *New England Journal of Medicine*, 360, 376–  
555 386, 2009.

556 Riipinen, I., Pierce, J. R., Donahue, N. M. and Pandis, S. N.: Equilibration time scales of  
557 organic aerosol inside thermodenuders: Evaporation kinetics versus  
558 thermodynamics, *Atmospheric Environment*, 44, 597–607,  
559 doi:10.1016/j.atmosenv.2009.11.022, 2010.

560 Saleh, R., Donahue, N. M. and Robinson, A. L.: Time scales for gas-particle partitioning  
561 equilibration of secondary organic aerosol formed from alpha-pinene ozonolysis,  
562 *Environ. Sci. Technol.*, 47, 5588–5594, doi:10.1021/es400078d, 2013.

563 Wehner, B., Philippin, S., and Wiedensohler, A.: Design and calibration of a  
564 thermodenuder with an improved heating unit to measure the size-dependent  
565 volatile fraction of aerosol particles, *J. Aerosol Sci.*, 33, 1087–1093, 2002.

566 Wehner, B., Philippin, S., Wiedensohler, A., Scheer, V., and Vogt, R.: Variability of non-  
567 volatile fractions of atmospheric aerosol particles with traffic influence, *Atmos.*  
568 *Environ.*, 38, 6081–6090, 2004.

569 Ulbrich, I. M., Canagaratna, M. R., Zhang, Q., Worsnop, D. R. and Jimenez, J. L.:  
570 Interpretation of organic components from Positive Matrix Factorization of  
571 aerosol mass spectrometric data, *Atmos. Chem. Phys.*, 9, 2891–2918, 2009.

572 Zhang, Q., Jimenez, J. L., Canagaratna, M. R., Allan, J. D., Coe, H., Ulbrich, I., Alfarra,  
573 M. R., Takami, A., Middlebrook, A. M., Sun, Y. L., Dzepina, K., Dunlea, E.,  
574 Docherty, K., DeCarlo, P. F., Salcedo, D., Onasch, T., Jayne, J. T., Miyoshi, T.,

575 Shimono, A., Hatakeyama, S., Takegawa, N., Kondo, Y., Schneider, J., Drewnick,  
576 F., Borrmann, S., Weimer, S., Demerjian, K., Williams, P., Bower, K., Bahreini,  
577 R., Cottrell, L., Griffin, R. J., Rautiainen, J., Sun, J. Y., Zhang, Y. M. and  
578 Worsnop, D. R.: Ubiquity and dominance of oxygenated species in organic  
579 aerosols in anthropogenically-influenced Northern Hemisphere midlatitudes,  
580 *Geophys. Res. Lett.*, 34, L13801, doi:10.1029/2007GL029979, 2007.

581 Zhang, Q., Jimenez, J. L., Canagaratna, M. R., Ulbrich, I. M., Ng, S. N., Worsnop, D. R.,  
582 and Sun. Y.: Understanding atmospheric organic aerosols via factor analysis of  
583 aerosol mass spectrometry: a review, *Anal. Bioanal. Chem.*, 401, 3045–3067,  
584 2011.

585  
586  
587

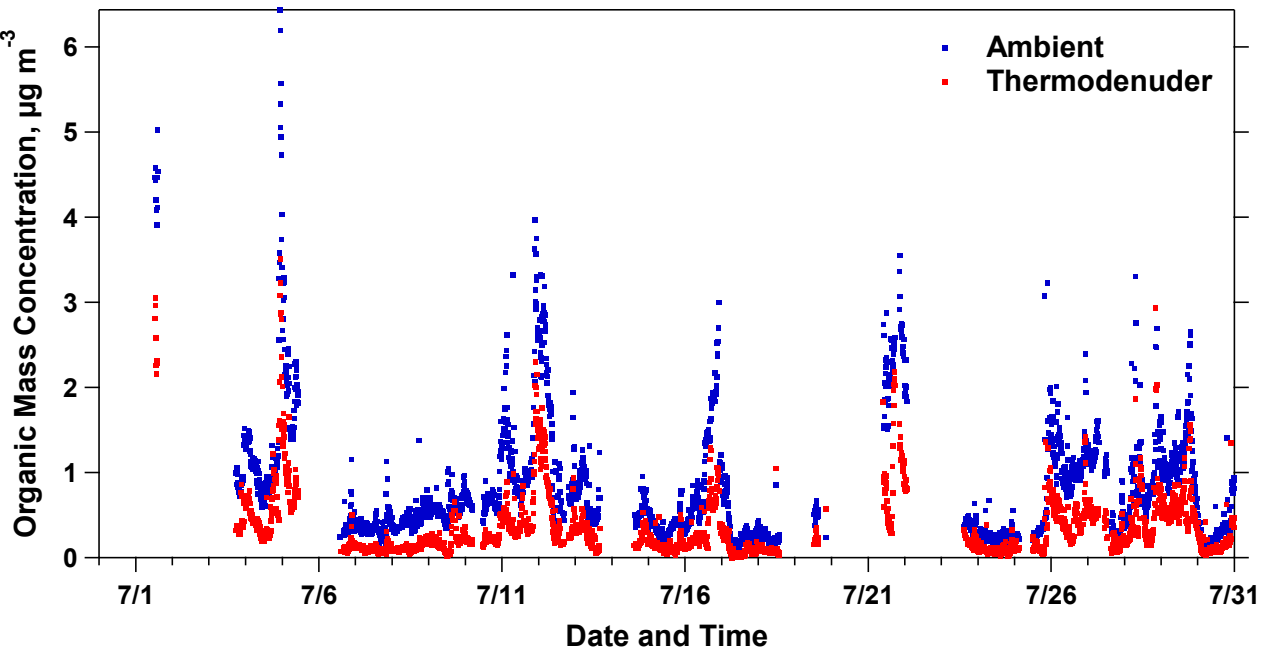
588  
589  
590

**Table 1.** Average and threshold ambient concentrations for each PMF factor.

<b>PMF Factor</b>	<b>Season</b>	<b>Average Mass Concentration (<math>\mu\text{g m}^{-3}</math>)</b>	<b>Threshold Concentration (<math>\mu\text{g m}^{-3}</math>)</b>	<b>Percentage of Measurements above Threshold</b>
HOA	Summer	0.16	0.08	53
COA		0.25	0.05	69
MOA		0.17	0.10	73
SV-OOA		0.65	0.10	82
LV-OOA		0.12	0.08	69
HOA	Winter	0.95	0.20	95
COA		0.48	0.08	92
BBOA		0.60	0.07	90
OOA		3.78	0.40	99

591  
592  
593  
594  
595  
596  
597  
598  
599  
600  
601  
602  
603  
604  
605  
606  
607  
608  
609  
610  
611  
612  
613  
614  
615  
616  
617  
618  
619  
620

621  
622  
623  
624  
625  
626  
627  
628  
629  
630  
631  
632  
633  
634  
635  
636  
637  
638  
639  
640  
641  
642  
643



644 **Figure 1.** Ambient (blue dots) and thermodenuder (red dots) organic mass concentration  
645 measurements for Paris during summer 2009.

646  
647  
648  
649  
650  
651  
652  
653  
654  
655  
656  
657  
658  
659  
660  
661  
662  
663  
664  
665

666  
667  
668  
669  
670  
671  
672  
673  
674  
675  
676  
677  
678  
679  
680  
681  
682  
683  
684  
685  
686  
687  
688  
689  
690  
691  
692  
693  
694  
695  
696  
697  
698  
699  
700

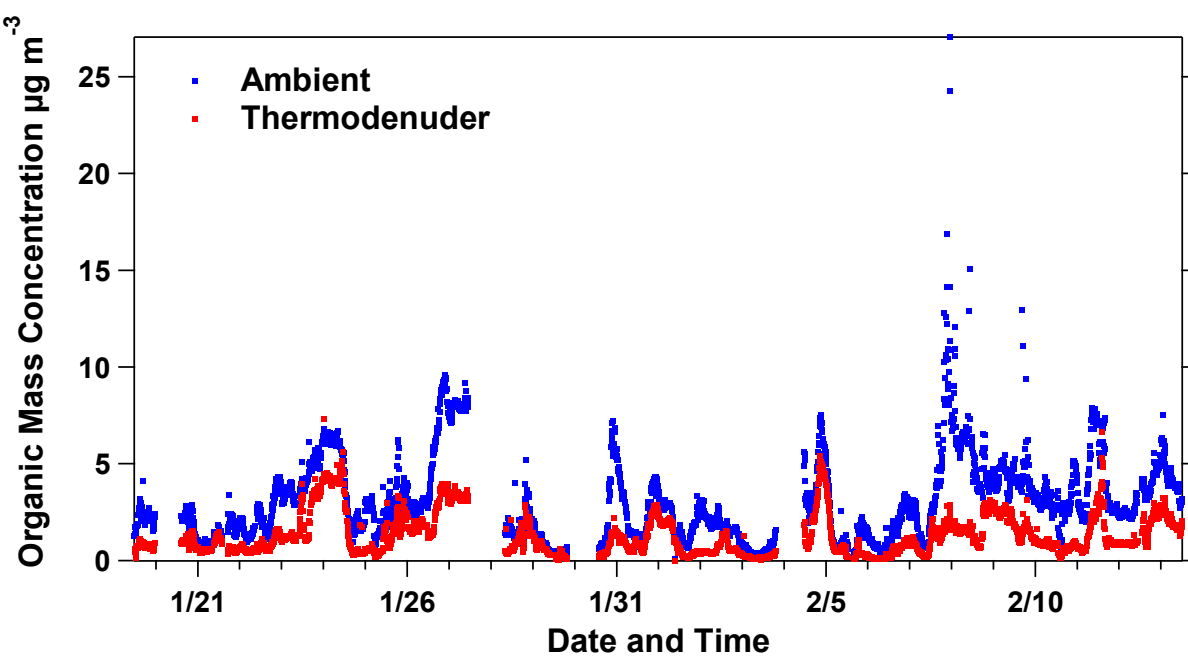
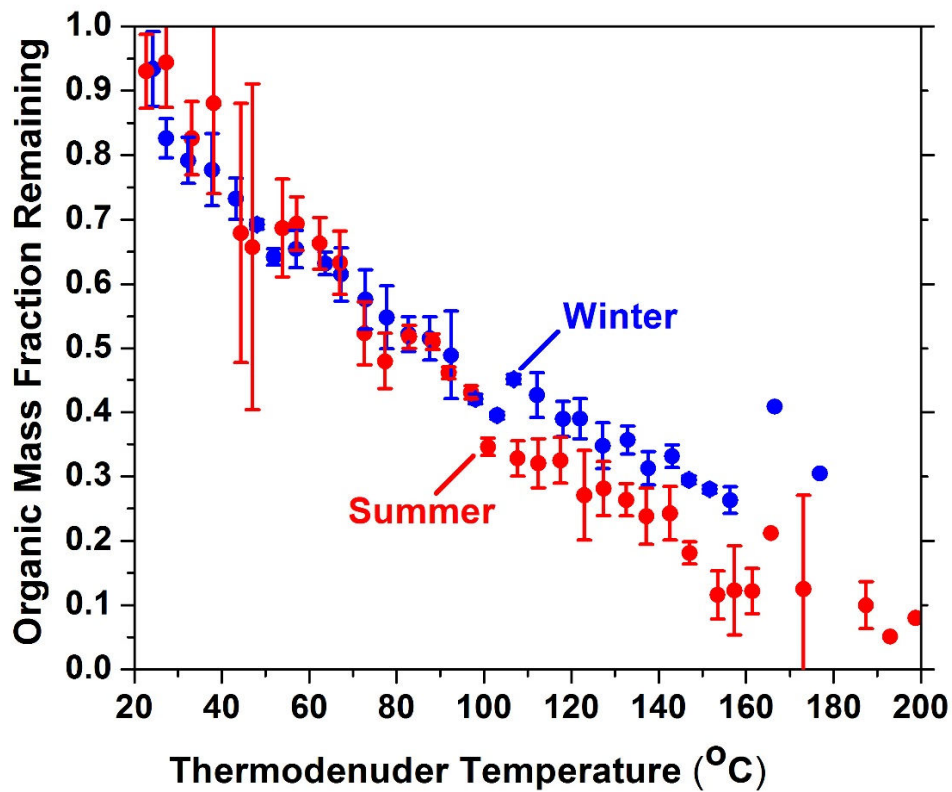


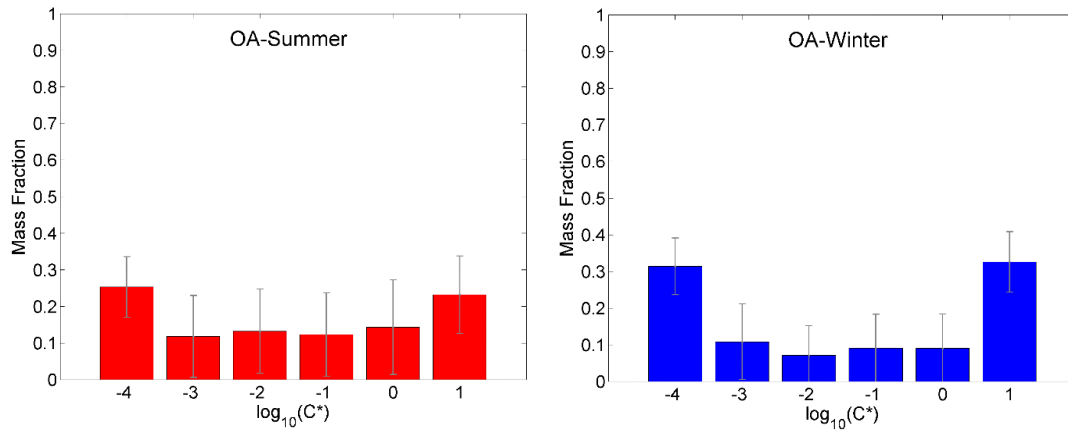
**Figure 2.** Ambient (blue dots) and thermodenuder (red dots) OA mass time series for the winter 2010 campaign.



701  
 702  
 703  
 704  
 705  
 706

**Figure 3.** Loss-corrected average OA thermograms for summer (red circles) and winter (blue squares) campaigns. The error bars correspond to plus/minus 2 standard deviations of the mean. Points with no error bars correspond to a single measurement.

707  
708  
709  
  
710  
  
711  
  
712



713 **Figure 4.** Estimated volatility distributions for summer (left panel) and winter total OA  
714 (right panel). The error bars correspond to the fitting uncertainties according to the  
715 algorithm of Karnezi et al. (2014).  
716

717

718

719

720

721

722

723

724

725

726

727

728

729

730

731

732

733

734

735

736

737

738

739

740

741

742

743

744

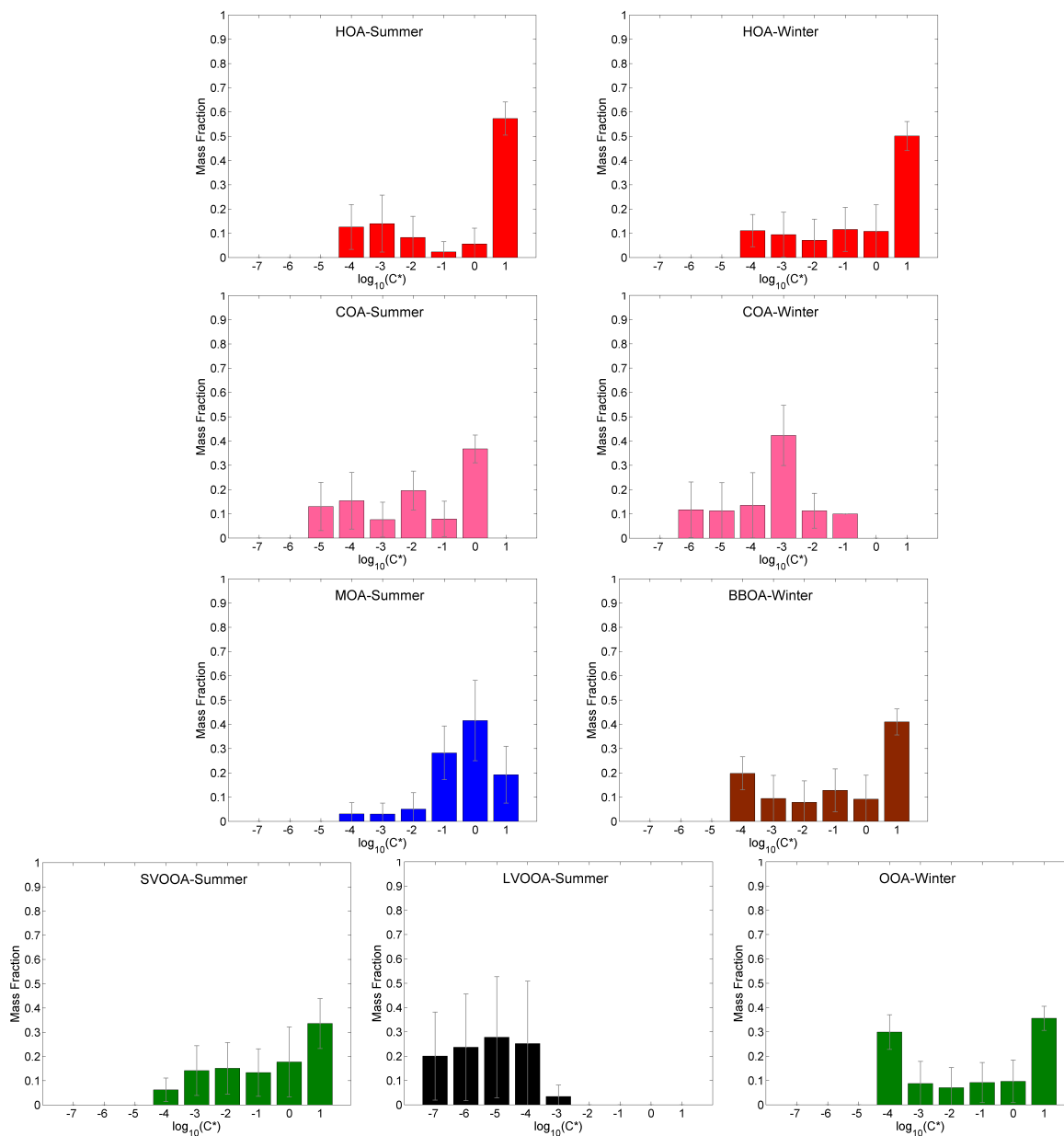
745

746

747

748

749



750 **Figure 5.** Estimated volatility distributions for summer PMF factors (left panel) and  
751 winter PMF factors (right panel). The error bars correspond to the fitting uncertainties  
752 according to the algorithm of Karnezis et al. (2014).

753  
754

755  
756  
757  
758  
759  
760  
761  
762  
763  
764  
765  
766  
767  
768  
769  
770  
771  
772  
773  
774  
775  
776  
777  
778  
779  
780  
781  
782  
783  
784  
785  
786  
787  
788  
789  
790  
791  
792  
793  
794  
795  
796

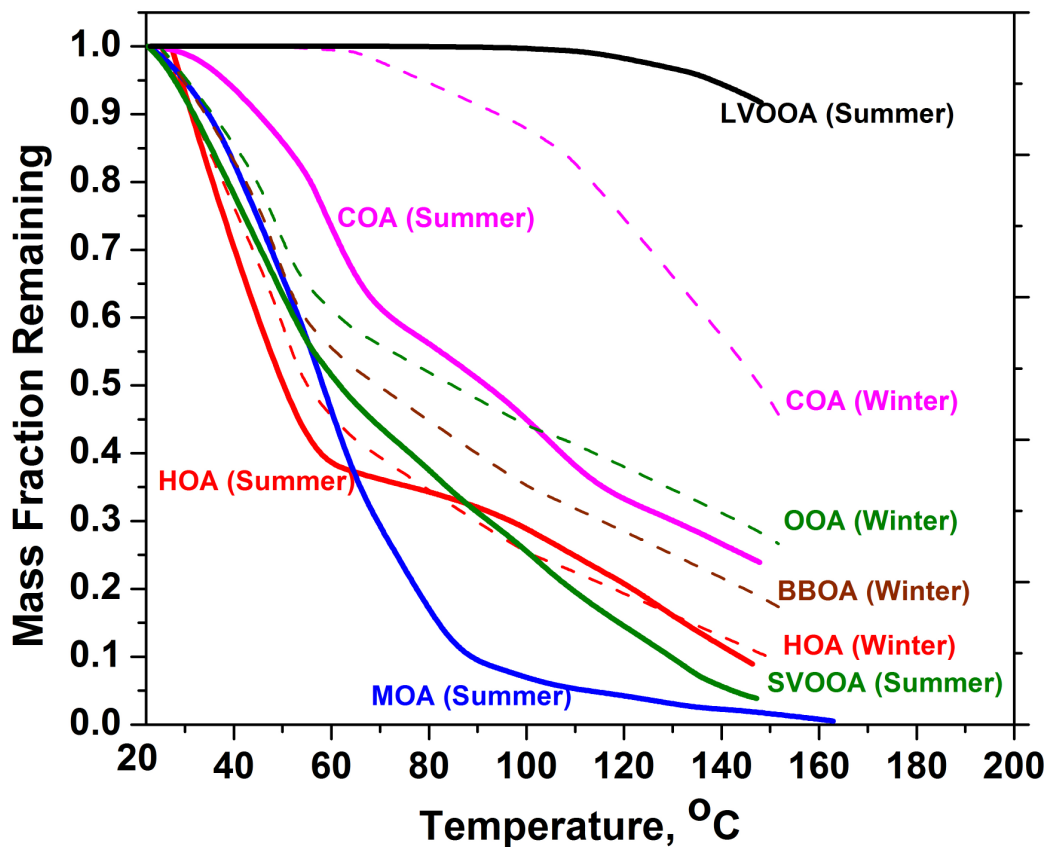


**Figure 6.** Estimated best-fit thermograms for all PMF factors. The solid lines represent the thermograms for the summer campaign and the dashed lines the thermograms for the winter campaign.

797  
798  
799  
800  
801  
802  
803  
804  
805  
806  
807  
808  
809  
810  
811  
812  
813  
814  
815  
816  
817  
818  
819  
820  
821  
822  
823  
824  
825  
826  
827  
828  
829  
830  
831  
832  
833  
834  
835  
836  
837  
838  
839  
840  
841  
842

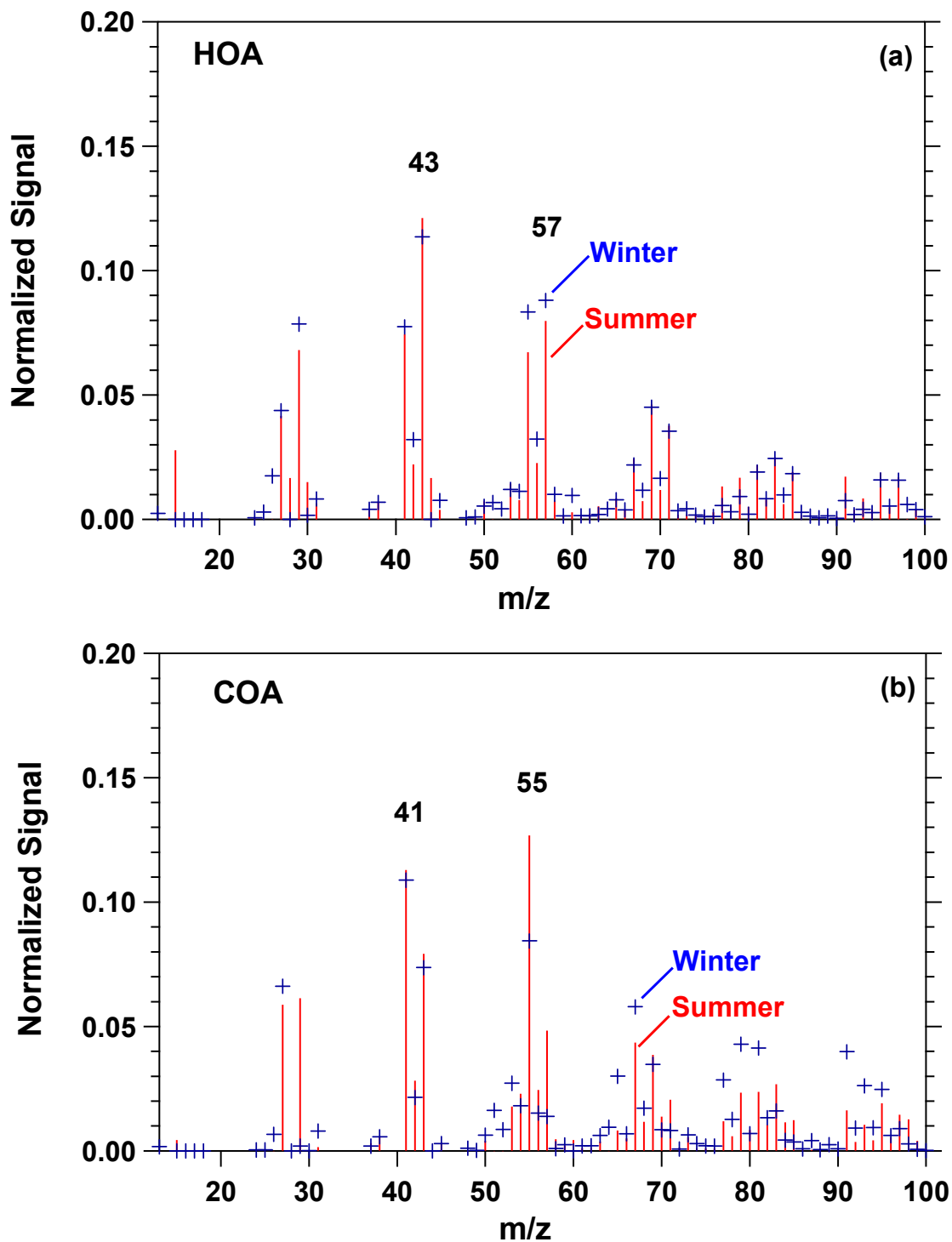


**Figure 7.** Seasonal mass spectra comparison for (a) HOA and (b) COA in Paris. Red lines correspond to the summer measurements while blue symbols correspond to the winter data.

843  
 844  
 845  
 846  
 847  
 848  
 849  
 850  
 851  
 852  
 853  
 854  
 855  
 856  
 857  
 858  
 859  
 860  
 861  
 862  
 863  
 864  
 865  
 866  
 867  
 868  
 869  
 870  
 871  
 872  
 873  
 874  
 875  
 876  
 877  
 878  
 879

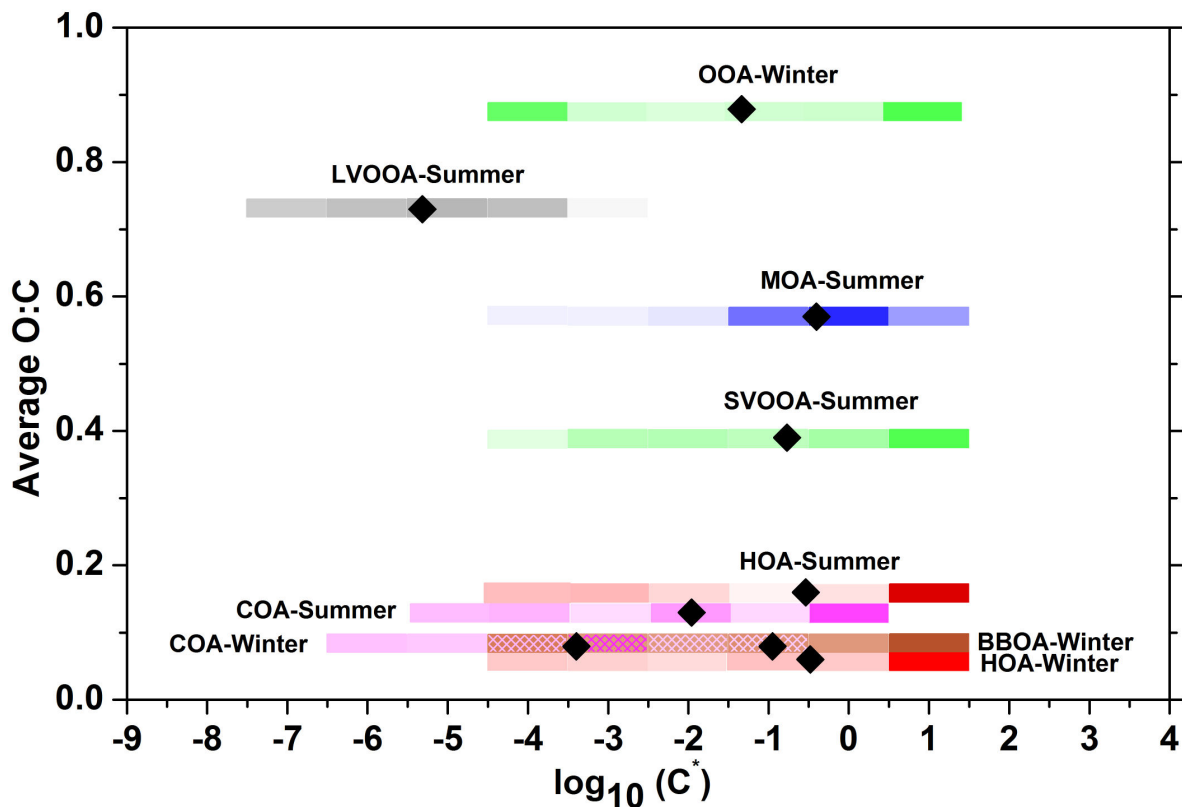


**Figure 8.** 2-D VBS representation of the PMF factors for the summer and winter campaigns. With the red color of the bars we represent the HOA factors, with the pink color the COA factors, the green the SVOOA and OOA, the blue is for the MOA factor, the brown for the BBOA factor and the black for the LVOOA factor. The darker shading of the colored bars denotes a larger mass fraction for a given  $C^*$  bin. The diamond represents the average  $\log_{10}(C^*)$  value for a given PMF factor.